



Soft Matter

Response of a raft of particles to a local indentation

Journal:	<i>Soft Matter</i>
Manuscript ID	SM-ART-06-2019-001251.R1
Article Type:	Paper
Date Submitted by the Author:	28-Jan-2020
Complete List of Authors:	He, Wei; University of Massachusetts Amherst, Physics Sun, Yiwei; University of Massachusetts Amherst, Physics Dinsmore, Anthony; University of Massachusetts, Physics

SCHOLARONE™
Manuscripts

Response of a raft of particles to a local indentation

Wei He, Yiwei Sun, and Anthony D. Dinsmore*

Department of Physics, University of Massachusetts Amherst

**E-mail: dinsmore@physics.umass.edu*

ABSTRACT

Interfaces that are coated with a layer of adsorbed particles (particle “rafts”) are common in natural and industrial settings. Particle-coated interfaces may be useful in part because the particulate structure can endow the fluid interface with physical properties distinct from molecular surfactants. We study the mechanics of particulate assemblies by measuring the raft’s response to indentation in the vertical direction by a flat, circular disc. We measured force (f) vs. indentation depth (δ) and found two linear regions with different slopes. The first linear region started at $\delta = 0$ and persisted over a range of δ much less than the capillary length. In the second linear region, the raft had the same stiffness ($df/d\delta$) as a liquid interface with no particles. Further, we show that, as long as the indenter was larger than a single particle, the azimuthal compression imposed by the interface deformation relaxed through in-plane rearrangement of particles rather than by the radial wrinkles that are characteristic of thin elastic sheets at fluid interfaces. We show how the force-displacement curves and stiffnesses depended on fluid mass densities, interfacial tensions, and indenter radius. For all cases studied, the particle-raft coated interfaces had a stiffness equal to or smaller than that of a bare fluid interface. Although the interfacial particle raft behaved like a pure fluid interface under a wide range of displacements, we show that the raft could nonetheless withstand substantially greater applied force (up to $2\times$) and greater indentation depth (up to $2.6\times$), so that the range of reversible behavior was greatly extended. These results improve our understanding of the mechanics of particulate assemblies at interfaces.

Introduction

Fluid interfaces that are coated by a layer of adsorbed particles occur widely in insect colonies,^{1,2} foods,^{3,4} particle separation technologies,⁵ oil-spill cleanup,⁶⁻¹³ and suppression of water evaporation in reservoirs.¹⁴ In solid-stabilized (Pickering) emulsions, solid particles adsorb onto the interface between the two phases and thereby prevent droplet coalescence; they find application in crude oil recovery and targeted drug delivery,^{6,10-13} among others. Similarly, particles can stabilize liquid-air interfaces, allowing the long existence of foams¹⁵ such as coffee crema,¹⁶ and “liquid-marble” droplets in air.^{17,18} In many of these examples, the mechanical response of the particle layer plays a crucial role in applications. In some examples, the particle-coated layer confers rigidity and allows non-spherical droplet shapes.^{17,19-22} In concentrated Pickering emulsions, the storage and loss moduli are likely to be influenced by the mechanical response of individual particle-coated droplets. It might also be the case that droplet breakup or coalescence are enhanced or suppressed with particle-laden interfaces, compared to surfactant-coated interfaces.

Early progress toward understanding particle-coated interfaces came from measurements of surface pressure-area isotherms of planar particle monolayers (rafts) on Langmuir troughs. Through compression-expansion cycles, this method captured the transition from a fluid interface to an elastic interfacial monolayer and the formation of wrinkles and folds.²³⁻²⁹ These studies showed wrinkles and a wrinkle-to-fold transition in rafts under uniaxial compression, which is analogous to (though not identical to) the behavior of thin elastic sheets.^{26,29} Additionally, the bending modulus of rafts was measured *via* static compression³⁰ or from propagation of surface waves,^{31,32} which show that the bending modulus scales as γa^2 , where γ is the interfacial tension and a is the particle radius. The stretching modulus has also been

measured from surface wave propagation; it scales with γ (independent of a), though the value of γ can be reduced by the presence of the particles.³¹

Response to a local indentation, however, differs from the above cases by inducing dilation in the radial direction and compression in the azimuthal direction. (Here we use polar coordinates, where the indenter's position defines the origin.) Owing to the azimuthal compression, indenting thin elastic sheets such as polymer films a few to hundreds of nm thick, leads to wrinkles that extend radially outward from the indenter.^{33,34} In these thin elastic films, the energy needed to bend and thereby form wrinkles is much less than the energy that would arise from in-plane compression.³⁵⁻³⁷ A natural question, therefore, is whether this continuum prediction applies also to particulate rafts, or whether the discreteness of the particles changes the response. For example, one might intuitively expect the strong particle-particle contact repulsion to make rigid-particle rafts stiffer than expected from continuum elasticity (at least under compression), or to be more prone to buckling out of plane. In recent experiments,³⁸ Zuo, *et al.* indented interfacial rafts of 16-nm-diameter particles with a vertically oriented rod and measured the resulting force-displacement curves. They found that the particle raft changed the effective contact angle on the rod, and that the raft-covered interface responded like a clean (raft-free) fluid interface with a modified contact angle. They also found that the particle raft greatly enhanced the maximum force that a water-air interface can sustain. These authors proposed that the particle raft was under tension, so that particles would be pulled apart from one another and inter-particle compression would be avoided. This explanation, though, does not consider that the stress field in the particle raft is non-uniform and non-isotropic and may include compressive components, so that contact repulsions might still be expected to play a role in stiffening the interface or causing buckling. Hence the mechanism by which rafts composed of discrete particles respond to applied normal indentation still needs to be addressed.

In this article, we report measurements of indentation of particle rafts bound at liquid/air or liquid/liquid interfaces. We pressed downward with a flat, circular indenter and measured the vertical force (f) and indentation (δ) while capturing top-view images to track the in-plane displacements of particles. We used combinations of air, water and oil with various values of mass density ρ and interfacial tension γ . The relative importance of gravitational and capillary forces acting on the interface is typically quantified by the capillary length, $l_c = \sqrt{\gamma/\Delta\rho g}$, where g is the acceleration due to gravity. Interfacial tension predominates at distances small compared to l_c and gravity predominates at much larger distances. In our experiments, l_c ranged from 2.72-18.35 mm. The particle radius (a) was 0.79 μm and the radius of the indenter (R_{in}) ranged from 2-10 mm. For $\delta \ll l_c$ but comparable to a , we found that f was linear in δ , so that there was a well-defined small- δ spring constant, which has not been reported previously. For larger displacements, we found a second linear regime with a stiffer spring constant $df/d\delta$. By formulating the measured $df/d\delta$ and δ in dimensionless form (in terms of R_{in} , γ and l_c), we found that our data collapsed onto a common curve in the second plateau regime. We conclude that in this regime, the effect of floating particles was negligible and the stiffness was determined by the bare-fluid interfacial tension, independent of the particles. Throughout the entire indentation process, we found that particles either had no effect on the interface stiffness or reduced it. These findings may seem counterintuitive, but we show that particles displaced radially inward in the plane of the interface to accommodate the compression without particle overlap, so that direct interactions between particles had a negligible energy cost compared to the capillary energy of increasing fluid-interface area. The resulting deformations led to a characteristic 6-fold star-

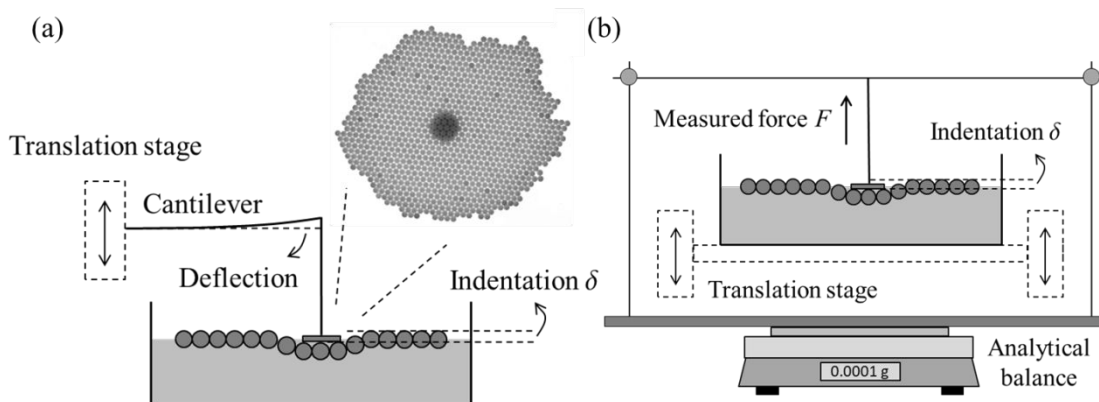


Fig. 1 Schematics of experimental setups. (a) Cantilever-based method. (b) Analytical balance-based method.

shaped pattern in hexagonal lattices, in which the measurable displacements were confined to a region of size comparable to l_c , smaller than the raft size. The particle raft did, however, increase the maximum depth that an indenter could reach before rupture, by at least a factor of 2.6 compared to a clean fluid/fluid interface. Rafts also increased the maximum force before rupture by at least a factor of two. In this way, the range of reversible loading and unloading was much greater with the raft. Finally, we discuss how these results should apply for particles that are micron- or nanometer-sized. Our conclusions shed new light on the response of particle rafts or particle-laden interfaces when both stretch and compression are present.

Experimental Methods and Materials

Fig. 1 shows the schematic of the two experimental setups with which we measured the response of a particle raft to normal indentation. In most experiments reported here, we used the cantilever-based method, shown in Fig. 1(a), to measure the force acting on a flat-bottom circular indenter. This method allowed simultaneous images of the raft from above and from the side. The indenter was attached by epoxy (ITW Devcon, no. 14277) to a metal needle, which was linked to a force-measuring cantilever. We found that plastic microscope slides (Fisherbrand, cat. no. S67112A) work well as the cantilever. Before each set of experiments, the cantilever stiffness was obtained by calibration measurements, in which loops of metal wire of known weight were placed at the end of the cantilever. Cantilever deflection was found to be linear with weight in the range of 0 to 27 mN, which spans more than the range of forces reported here. We obtained a typical force resolution of 8 μN . The lab temperature on different days varied in the range of 22–25 $^{\circ}\text{C}$.

As an alternative method, we measured the force directly with a precision of 10 μN using an analytical balance as shown in Fig. 1(b). The position of the indenter was fixed while the container was placed on a movable stage. In experiments, we displaced the container upward with a translation stage, and the contact force between the particle raft and the indenter was obtained from the change of the balance readout. This method did not allow for simultaneous imaging.

In all cases, the depth of the indenter (the “indentation,” δ) was defined as the distance between the bottom of the indenter and the top of unperturbed floating particles. The point where

$\delta = 0$ was set as the vertical position where the indenter first touched the particle raft when pushing downward. Downward f and δ were defined as positive. For the cantilever-based setup, δ was measured by image analysis with a precision of 15 μm , which was mainly limited by the resolution of the camera. For the analytical balance, the vertical position of the container was controlled by a translation stage, the precision of which was 5 μm . The indenter radius, R_{in} , varied from 2-6 mm in the data shown here. The sample container was circular with an inner diameter of approximately 145 mm. When the indenter pushed downward, the fluid level rose slightly because the fluid was incompressible. However, because R_{in} was much smaller than the container size, this change in level was smaller than δ by a factor of 200-1,500. In our analysis, we disregarded this small upward displacement.

We formed particle rafts from polymer spheres that bound at liquid/air or liquid/liquid interfaces. These particles were purchased from McMaster-Carr and Engineering Laboratories, Inc.: acrylic (radius $a = 1/32'' = 0.79$ mm, $\rho = 1,190$ kg/m³, cat. no. 1383K41), polytetrafluoroethylene (Teflon; $a = 1/32'' = 0.79$ mm, $\rho = 2,130$ kg/m³, cat. no. 9660K11) and polystyrene ($a = 1/32''$, $\rho = 1,040$ -1,060 kg/m³). Acrylic particles were washed in deionized water and then dried before each set of experiment. Other particles were cleaned by sonicating in methanol, rinsing in deionized water, and then drying in air. Measured advancing contact angles at water-air interfaces for particles of Teflon, polystyrene, and acrylic were $104 \pm 5^\circ$, $90 \pm 5^\circ$, and $77 \pm 5^\circ$. The indenter had an advancing angle of roughly 120° .

The liquids used in the experiments were deionized water (Milli-Q plus) with a surface tension of 72 mN/m, two different types of silicone oil with density of 0.96 g/mL and 1.05 g/mL (Sigma-Aldrich, cat. no. 146153 and 175633, respectively), squalane with density of 0.81 g/mL (Sigma-Aldrich, cat. no. 234311) and hexadecane with density of 0.77 g/mL (Sigma-Aldrich, cat. no. 105168). In some experiments, a mixture of silicone oil and hexadecane was used to minimize the density mismatch of two liquid phases. The mass and volume of oil mixtures were measured using an analytical balance and a volumetric flask. The density of the fluid was then calculated. The interfacial tensions of the oil mixture and of water were measured using a pendant droplet tensiometer (OCA 20, Future Digital Scientific Co., Garden City). All experiments were performed at room temperature.

Spheres were placed by hand on the liquid/liquid or liquid/air interfaces. They formed a two-dimensional hexagonal lattice owing to inter-particle capillary attraction, known as the Cheerios effect.^{39,40} Typical raft sizes were approx. 800-2000 particles (corresponding to diameters of about 50-80 mm). We manually arranged the lattice to make the raft approximately circular. The rafts reported here were cohesive: they maintained their size and shape when left alone at the interface. To minimize the boundary effect from the edge of the sample container, we made sure that the edge of the container was at least $5 \times l_c$ away from the edge of the particle raft in all experiments.

In a typical experiment, we started with the probe above the raft and then lowered it (or raised the container) by a fixed vertical displacement. The height of the probe (or the container) was adjusted manually using the translation stage. After each vertical displacement, the system was allowed to relax for 15 s, after which we saw no additional changes in the particle layer or in f or δ . The values of f and δ were recorded. This procedure was repeated until the raft was broken (caused by wetting of the indenter and clearly visible by a complete disruption of the raft's structure). Between each set of experiments, the indenter was cleaned and dried, and the raft was restored to its initial state manually.

Results and discussion

Fig. 2 shows an overview of our measured $f(\delta)$. Six example experiments are shown, performed on different kinds of fluid/fluid interfaces (water-air, water-squalane and water-hexadecane/silicone oil mixture) with various values of probe radius R_{in} and capillary length l_c . The ratios R_{in}/l_c varied from 0.59 to 2.21. We used Teflon or acrylic particles at water-air interface and polystyrene particles at water-oil interfaces. Most experiments were repeated multiple times and the results were indistinguishable. Starting from the moment that the probe just touched the particle raft, the measured force was always positive and monotonically increased. Immediately after the final data point for most traces, the indenter ruptured the interface and the raft was destroyed.

Although some of the f - δ curves are close to straight lines, a close look shows that their slopes varied throughout the experiment. To highlight this nonlinear feature, the inset of Fig. 2 shows an example of $df/d\delta$ vs. δ measured for a polystyrene-particle-raft on a water-hexadecane/silicone oil mixture interface with $l_c = 10.2$ mm. The derivative at each point was calculated by a moving average with a window containing three data points. Initially, $df/d\delta$ remained constant at approximately 0.195 mN/mm (dashed line) over a range of δ from 0-0.6 mm (equivalent to 0-0.2 l_c or 0-0.76 a). Meanwhile, top-view images showed no discernible in-plane displacement of the particles. We refer to this regime as the “first plateau.” Comparing the results for different fluids, we found that the range of δ in this plateau increased with l_c , though we could not identify a clear functional dependence. As shown in the inset of Fig. 2, the value of $df/d\delta$ increased with δ and then reached a new δ -independent value of approx. 0.32 mN/m with random noise (which we attribute to the numerical computation of the derivatives). This “second plateau” persisted over a few millimeters in δ . During this stage, nearby particles were pulled towards the indenter and a star-shaped pattern gradually became observable from above, as will be discussed below. Finally, $df/d\delta$ decreased and then (just beyond the last data point shown) the raft ruptured. As will be discussed below, these same features were found in all of our measurements of rafts with various combinations of parameters (Fig. S1), provided that $R_{in} \geq 2.5a$. When $R_{in} \approx a$, we found a different response that will be described below.

The first plateau, $\delta \ll l_c$

We begin our detailed discussion with the first plateau region. Because γ and l_c set the energy scale and the characteristic length-scale of the fluid interface shape,

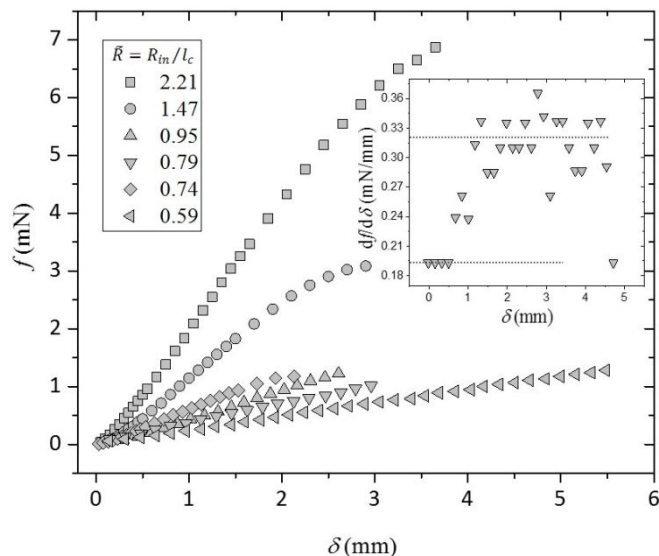


Fig. 2 Measured force, f , versus indentation, δ , for different combinations of particles, liquids and probes. Inset: $df/d\delta$ versus δ for a water-oil interface with $R_{in}/l_c = 0.79$. This plot shows a 1st plateau at small δ and a 2nd plateau over a range of δ of approximately 1.2-4.5 mm.

we extracted the first-plateau $df/d\delta$ values from different samples, normalized by γ , and plotted them against R_{in}/l_c (Fig. 3). Each experiment was repeated three or more times and the resulting statistics were used to obtain mean and standard error of the mean. The plot shows that all of our data collapse to a consistent trend, in which $(df/d\delta)/\gamma$ is proportional to R_{in}/l_c . The dashed straight line in the figure is a linear fit to the data, which has a slope of 5.5 ± 0.3 and a y -intercept of 0.7 ± 0.2 .

To explore the mechanism behind this first plateau, we made a particle raft with a size similar to the size of the indenter, and repeated the measurements on the same interface (water-air, $l_c = 2.7$ mm, Teflon particles). The resulting $df/d\delta$ were indistinguishable over the full range of δ for large and small rafts, indicating that the free-floating particles

outside the indenter region played no discernible role in f (Fig. S3). We also measured $f(\delta)$ at a clean (particle-free) fluid interface. At a clean interface, we found linear response extending from $\delta=0$ with a value of $df/d\delta$ that was indistinguishable in value from the second plateau of the raft: there was no separate plateau at small δ (Fig. S4).

The force applied by a clean fluid interface, which we call f_{clean} , can be calculated using standard capillary theory in the regime where the interface slope is small. The result (ESI Section I) is:

$$f_{\text{clean}} = 2\pi\gamma\tilde{R}\frac{K_1(\tilde{R})}{K_0(\tilde{R})}\delta + \pi\gamma\tilde{R}^2\delta \quad (1)$$

where K is the modified Bessel function of second kind and $\tilde{R} = R_{in}/l_c$. The first term is the capillary force applied by the fluid-fluid interface on the edge of the indenter and is proportional to the circumference of the indenter, and hence linear in \tilde{R} . The second term accounts for the hydrostatic pressure on the indenter's surface.⁴¹ This term includes the weight of the displaced fluid and accounts for the different densities of the upper and lower phases; this term is proportional to \tilde{R}^2 . From Eqn (1), we found $(df/d\delta)/\gamma$ and plotted the result as the dotted curve in Fig. 3. This model does not agree with the data so it cannot explain the first plateau.

In Fig. 3, the linear scaling and the absence of a quadratic (\tilde{R}^2) component suggest that the capillary force acting on the particles underneath the indenter's rim dominates the behavior in the first plateau region. We therefore plotted only the capillary component of Eqn. (1) (the solid curve in Fig. 3), but the measured values are still much smaller *i.e.*, softer than a clean interface. Although we are unable to account quantitatively for the experimental data, we propose that the first plateau arises from contact-angle hysteresis on the particles, and/or the fact that the 3-phase

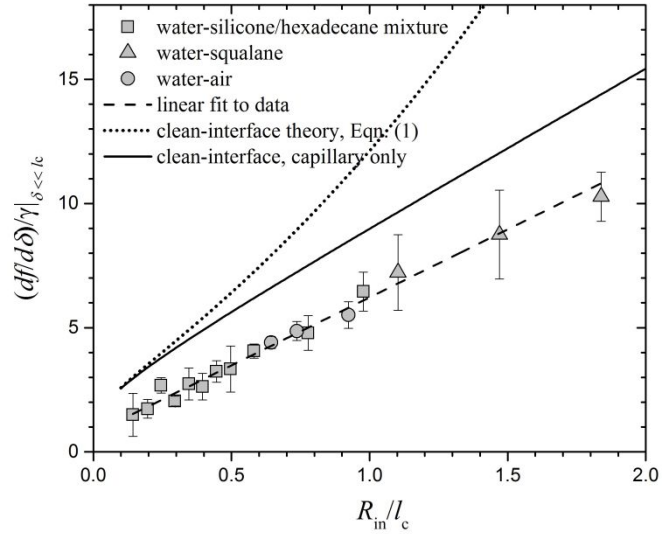


Fig. 3 The normalized derivative, $(df/d\delta)/\gamma$, in the first plateau region, where $\delta \ll l_c$. Several measurements of different rafts with different particle types are shown. Error bars show the standard error of the mean of multiple measurements. The dashed line is a linear fit to the data. The dotted line is the clean-interface theory (Eqn. 1) and the solid curve is just the first (capillary) term of Eqn. (1).

contact line for the raft undulates around the particles, whereas for a clean interface it is a smooth circle. In earlier measurements of capillary forces on a spherical particles, we found that a deformed or undulating contact line generically reduced the capillary force on the sphere.⁴² The geometry is different here but a similar mechanism may be at play. The absence of any measurable component that scales with \tilde{R}^2 suggests that the fluid interface itself was not significantly pushed downward. Instead, it may be that the indenter only pushed particles deeper into the liquid until the three-phase contact line reached the advancing contact angle, beyond which point the interface moved down and the first plateau ended. (In the previous section, we noted that the upward displacement of the fluid caused by pushing the particles downward was much smaller than δ because the indenter was much smaller than the container.)

The second plateau, $\delta \approx l_c$

The inset of Fig. 4 shows measured $df/d\delta$ in the second plateau region, normalized by γ , vs. R_{in}/l_c for many different samples. (This plot is the second-plateau counterpart of Fig. 3.) The theory of Eqn. (1) is shown as the dotted curve and the agreement is excellent. We also found that the data are accurately fit by a second order polynomial (dashed curve). The coefficient of the quadratic term is 3.78 ± 0.5 , which is close to the value of π that is anticipated from the hydrostatic term in Eqn. (1). To remove the hydrostatic pressure and isolate the capillary forces, we subtracted $\pi\tilde{R}^2$, the second term of (Eq. 1), and plotted the result in the main panel of Fig. 4. We found that the capillary component of measured stiffness scaled consistently with R_{in}/l_c for three different interfaces and with R_{in}/l_c varying by a factor of approximately 13.

The solid black line in Fig. 4 is the pure-capillary component from Eqn. (1). We found that the data points agree with the theoretical curve, showing that the particle raft's second-plateau stiffness is indistinguishable from the clean fluid interface. This point was also demonstrated in two other ways: by plotting the full $f(\delta)$ curves in rescaled, dimensionless form and comparing to theory (Fig. S2), and by direct comparison of a raft and a clean-interface (Fig. S3).

In other words, the response of the system to a local mechanical load is effectively fluid-like rather than solid-like. This is a key result of these studies. In the conclusion section, we compare our measured stiffness to prior theory for thin, continuous elastic sheets with low bending modulus.

We emphasize that the measured stiffness in the second plateau regime was set by the measured bare-fluid interfacial tension, γ . We did not find some effective γ reduced by the presence of particles. Previous work showed that if there are excess particles in suspension (so that more particles can bind when more area is exposed), then the effective interfacial tension is lowered by the particle binding energy.⁴³ In the present case, however, the number of particles was fixed so that stretching led to new, clean fluid interface. These results apparently differ from

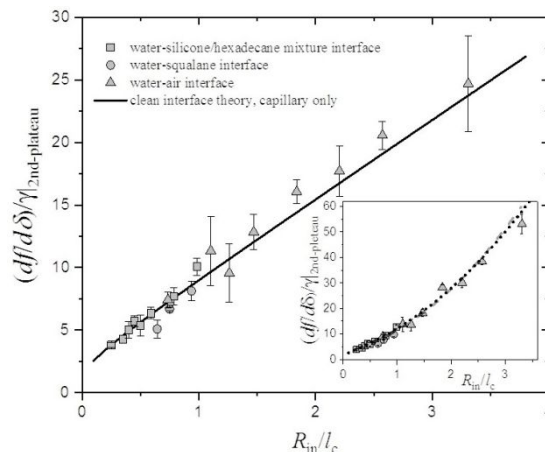


Fig. 4 The normalized derivative, $(df/d\delta)/\gamma$, in the second plateau region, where $\delta \sim l_c$. Results for several different rafts are shown. In the main plot, the hydrostatic part of the force was subtracted and the solid curve is the first (capillary) term of Eq. (1). The inset shows the derivative of original data, using the total measured f . The dashed curve is a best-fit second-order polynomial and the heavy dotted curve is the theory of Eq. (1).

previous measurements of the stretching modulus of particle rafts (spherical glass particles, 0.03-0.15 mm diam.) made *via* wave propagation;³¹ that report found a stretching modulus that was 20% smaller than the pure-fluid interfacial tension. There, the reduced stiffness was attributed to particles that were initially slightly out of plane, which could then settle into the interface during expansion and reduce the effective interfacial tension. In the present experiments, the particles were sufficiently large that we could ensure that all of them sat at their steady-state position astride the interface before the indentation experiments began.

To investigate whether hexagonal order is important, we intentionally introduced packing defects in rafts by mixing particles of two different sizes and measured $f(\delta)$. An example is shown in Fig. S8. We found that the 1st-plateau regime stiffness was altered, likely because the indenter touched the larger particles first. The existence and the stiffness-value of the 2nd-plateau, however, were not distinguishable from the ordered rafts.

The fact that the particle raft does not contribute to the stiffness of the interface strikes us as counterintuitive. Indeed, at the start of these experiments, we anticipated that the particles would make the interface stiffer because of their cohesion and because we anticipated compression in the azimuthal direction. We therefore turn now to the question of why a cohesive particulate layer would have no effect on the stiffness against indentation. The key is to look at in-plane displacements.

In-plane particle displacements

Indentation led to a characteristic 6-fold symmetric, star-shaped pattern of particle displacements shown in Fig. 5(a). These patterns were only visible in the 2nd-plateau region; we could not discern any in-plane particle displacements in the 1st-plateau regime (Fig. S5). The points of the star aligned with the $\langle 11 \rangle$ crystal directions, 30° away from the close-packed lattice direction.

In each pattern, there were no discernible displacements at radial distances beyond a characteristic cutoff value that increased with l_c and R_{in} . This observation differs from experiments of Jambon-Puillet, *et al.*,⁴⁴ who found that particles at the raft's edge displaced. In the present experiments, we attribute the lack of displacement at the edge to the large size of the raft compared to l_c , whereas the earlier study had rafts comparable in size to l_c . (In our experiments we did, however, observe inward displacements at the edges of rafts at mixed-oil/water interfaces where the raft size was comparable to l_c (Fig. S7). We suspect that the cutoff range depends on l_c because it sets the scale for deformations of the interface.)

The deformations were reversible: when we halted the indentation before the indenter was wetted by the lower liquid phase, and then raised the indenter, we found that particles returned to their original locations for air-water interfaces. During the reversed (lifting) process, the force curve was offset to smaller force values, presumably because of hysteresis of the contact angle on the particles (Fig. S9).

In Fig. 5(a), the camera image shows a projection of the particles onto the horizontal plane, while the interface itself was curved. However, the star-shaped pattern was not merely an artifact of imaging a curved surface. One way to tell this is to note the sizeable gaps between particles that appear near the “tips” of the points of the star (see white dashed circles in Fig. 5(a)). Assuming that the interface shape was the same as that of a clean interface (see SI), we numerically estimated the slope at these points and found that the interface was nearly horizontal there (slope < 0.08). Thus, the projected particle separation and the true separation (measured along the interface) differed by less than 0.3% and the distortion from the curvature was too

small to alter the qualitative pattern. Close to the indenter, the slope increased to near 0.5 and the projected separation was about 10% smaller than the true separation.

To explain why the star-shaped displacement patterns appeared, we first consider what would happen if the particle displacement field were isotropic, independent of azimuthal angle. In such a case, the downward displacement δ would cause radially inward displacement of the particles, which is indeed the case here (Fig. 5(a,b)). In the azimuthal direction, this inward displacement should cause compression, owing to the fact that each inward-displaced ring of particles would have a smaller circumference. Because of the high modulus of these particles, this compression should be energetically prohibitive. A possible way to relax the azimuthal compression is to form wrinkles, as occurs in an elastic sheet.³³ Wrinkles would effectively increase the perimeter of each ring of fixed radius so that the particles could avoid overlapping one another. In all our experiments, however, we could discern no out-of-plane displacements of the particle raft.

We can clarify the mechanism for the star-shaped pattern by modeling the raft as an ideal close-packed lattice of hard spheres, which are constrained to lie along the fluid interface.

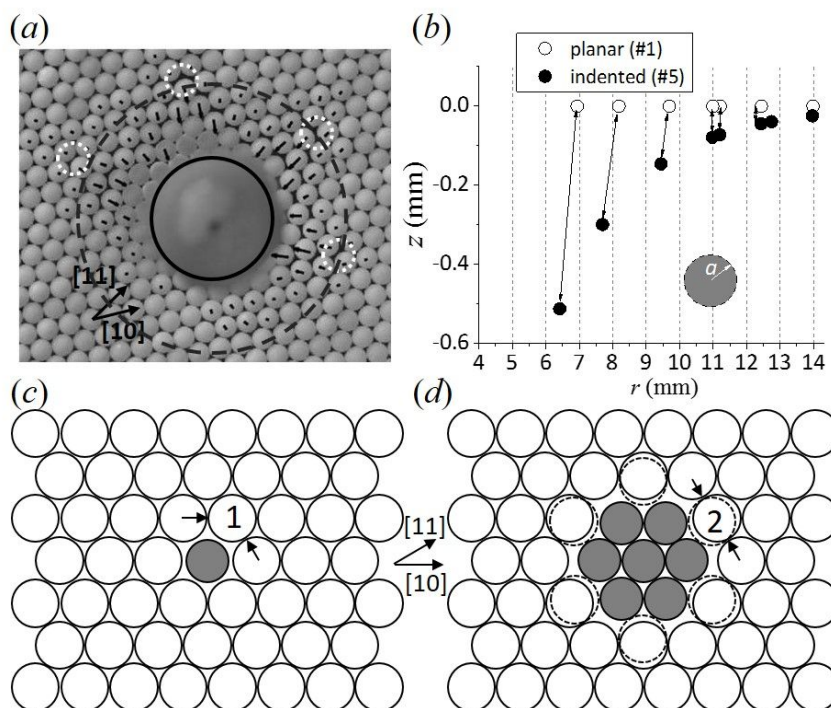


Fig. 5(a) Top-view image of PTFE particles with $a = 0.79 \pm 0.05$ mm, $R_{in} = 4$ mm, and $\delta/l_c = 0.49$, which is in the second plateau regime (configuration #5 of Fig. S5). Superimposed on the image are the projected particle displacements relative to the initial lattice, magnified 10 \times . The overlaid black circle shows the boundary of the indenter. The dashed gray ring shows, roughly, the boundary within which we could discern deformation. (b) Plot of the measured radial positions (r) of centers of the particles in two configurations (#1,5 of Fig. S5, with $\delta = 0, 1.33$ mm) in the angular range $0.8 < \theta < 1.0$ rad. The heights z were calculated by assuming that the interface shape was the same as a bare fluid interface, as described in the text. The downward displacement of the indenter led to radially inward particle displacements. (c) Illustration of indenting a single particle, shown in gray. The neighboring particles (such as that labeled 1) cannot move inward because of the contact repulsion from neighbors (arrows). (d) Illustration of indenting seven particles. Here, six of the surrounding particles (such as the one labeled 2) can move inward without hindrance from their neighbors. These six directions are the [11] and the 5 other similar ones (*i.e.*, $\langle 11 \rangle$). These directions correspond the tips of the star pattern in (a), shown by the white dashed circles.

Consider first the case of an indenter that pushes on just one particle (Fig. 5(c)): because of the jammed structure, none of the neighboring particles is free to move radially inward without first displacing its neighbors. In such a case, the indenter simply punches a hole in the raft without affecting the structure of the lattice. The result is quite different when we consider a hypothetical indenter with $R_{\text{in}} \approx 3a$, which covers seven particles (Fig. 5(d)). As these seven particles are pushed downward, the six particles labeled by arrows can freely move radially inward without hard-core repulsion from their neighboring particles. Once these six particles move, their neighbors can also move closer to the origin *and* closer to one another in the azimuthal direction without hard-core repulsion. These motions allow the lattice to accommodate azimuthal compression without out-of-plane wrinkles, and thus without increasing the fluid interfacial area.

To see whether displacements along the interface could relieve compression, we investigated the positions of particles in 3D. To do this, we first assumed that the indented surface had the same shape as a clean fluid interface (Eqn. (S5)). This assumption is indirectly supported by our observation that the capillary force is the same for the raft and for the clean interface. We further assumed that the particles remained bound to the interface. Within these assumptions, we calculated the height z of the particles in a wedge-shaped region that included one of the point of the star pattern. The results are shown in Fig. 5(b). We found that the particles in the indented raft tended to move radially inward and the inter-particle separations increased in the radial direction. By contrast, the separations in the azimuthal direction remained close-packed. Details may be found in the supplemental Fig. S10(b). These results are consistent with our model.

In our force measurements, we only found the first and second plateau behavior when we used indenters with $R_{\text{in}} \geq 2.5a$. By contrast, when $R_{\text{in}} \approx a$, the shape of $f(\delta)$ was very different: it decreased monotonically because of a continual change in the three-phase contact line and there was no plateau in $df/d\delta$.⁴² This result is again consistent with the proposed mechanism of Fig. 5(c,d).

We have argued that initially planar interfaces with free-floating particle rafts should not wrinkle under normal indentation. The in-plane deformation mechanism should predominate as long as the inter-particle forces are weak or of short range, so that the energy of creating the in-plane spacings is smaller than the capillary energy of out-of-plane wrinkling. Using the image of the disordered raft of Fig. S8, we found that the in-plane radial displacement mechanism can also reduce azimuthal compression, though a star-shaped pattern would not be expected. Interfaces with close-packed particle rafts that start under radial compression, however, might behave quite differently if the star-shaped deformation pattern cannot relieve enough compressive strain; it would be interesting to see whether such rafts would form out-of-plane wrinkles.

Maximum displacement and force

We measured the maximum depth that the indenter could reach and the maximum force the raft could sustain before rupture. Rupture occurred when the particles moved away from the indenter's rim and the indenter was wetted by the lower liquid phase. The resulting meniscus rapidly pushed nearby particles out of place and destroyed the raft. We never saw particles sinking into the bulk fluid in the oil-water experiments, and rarely saw this in the air-water experiments. Prior to rupture, the $f(\delta)$ curve could be repeated; beyond rupture it could not.

Figure 6 shows the maximum indentations and forces with Teflon-particle rafts at water-air interfaces ($l_c = 2.7$ mm) and with R_{in} ranging from 0.74 - 2.2 l_c . For comparison, we also plotted the maximum indentation and force for the same indenter at a clean, particle-free interface. With the help of the particle rafts, the interface was able to accommodate approximately $2\times$ larger

poking force and up to $2.6\times$ larger indentation before rupture. Indentation as large as $1.7 l_c$ were obtained for the larger R_{in} . In this way, the particle raft provided an effective mechanical protection to the interface, making it substantially tougher. At the clean interface, the contact line slipped past the rim and onto the top of the indenter once δ was large enough, and this led to immersion of the indenter. With the raft present, the particles just outside the indenter pinned the contact line more effectively than did the flat indenter.

Conclusions

In summary, we measured the response of rafts of particles adsorbed at planar liquid/air or liquid/liquid interfaces under a vertical indentation by a disc-shaped probe. In all cases where $R_{in} \geq 2.5a$, we found that the stiffness was equal to or less than that of a particle-free (clean) fluid interface, but that the particles allowed substantially deeper indentation ($2.6\times$) and greater maximum force. We also showed that there exist two regimes of linear response, or “plateaus” in the plot of $df/d\delta$.

When $\delta \ll l_c$, in what we call the first plateau region, the interfacial monolayer stiffness was substantially lower than that of a pure fluid interfacial tension. This low-stiffness regime typically persisted over a range of indentations much less than l_c and less than but comparable to a . For all systems studied, the first-plateau stiffness was approximately $(0.7 \pm 0.2) \gamma + (5.5 \pm 0.3) \gamma \tilde{R}$, where $\tilde{R} = R_{in}/l_c$ (Fig. 3). We speculated that the linear dependence on \tilde{R} arose from the undulated shape of the three-phase contact line at the indenter’s rim but we are unable to account for the constant offset or the coefficient of \tilde{R} .

In the higher- δ , second plateau region, the particle raft had the same stiffness $df/d\delta$ as a clean liquid interface, without particles. (The force itself, however, is slightly lower because of the first-plateau stiffness was smaller.) This similarity to clean interfaces was confirmed by direct experimental comparison and also by agreement with the predicted clean-interface stiffness, $2\pi\gamma\tilde{R} \frac{K_1(\tilde{R})}{K_0(\tilde{R})} + \pi\gamma\tilde{R}^2$ (Eqn. 1). With still deeper indentation ($\delta \sim l_c$), the stiffness decreased owing to the particle displacements up around the edge of the indenter.

We showed that as long as the indenter covered seven or more particles ($R_{in} \gtrsim 2.5a$), the imposed azimuthal compression was relaxed through a characteristic six-fold star-shaped pattern; no out-of-plane wrinkles were observed. We propose that the pattern of radially inward displacements (radial dilation) provided a low-energy mode of in-plane deformation, which allowed the raft to accommodate the imposed deformation without higher-energy particle overlap or discernible out-of-plane motion (Fig. 6a). Compared to spring-bonded systems, the relatively short range of inter-particle attractions in these rafts means that these radial displacements have much weaker energy cost, so that the star-shaped pattern appeared at relatively small indentation. For a small indenter with $R_{in} \approx a$, we

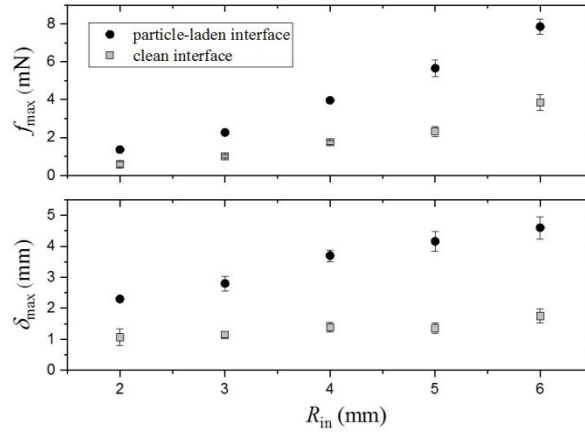


Fig. 6 Maximum force and maximum indentation before the rupture of the interface for different R_{in} at a water-air interface. Filled symbols correspond to indentation of a raft and open symbols correspond to indentation of a clean interface.

found that $f(\delta)$ was altogether different from the preceding discussion⁴² and we argued on the basis of geometry why the low-energy, in-plane star-shaped deformation is prevented in this limit.

Although we focused mainly on hexagonally ordered lattices of particles, the overall behavior was quite similar for disordered rafts, except for the quantitative scaling of the first-plateau stiffness. The mechanism of relaxing azimuthal compression by in-plane radially inward displacements also works for disordered rafts composed of circular or spherical particles.

Our results are distinct from a recent prediction of the stiffness against normal deformations, in which the interface was assumed to remain planar while the particles were pushed inward.⁴⁵ By this model, the stiffness scaled with R_{in}^2 divided by the area per particle on the interface. In terms of magnitude and parameter scaling, our results differ at all δ , presumably because the energy contribution from the deformed interface is always important in our experiments.

Our results share some of the features found by Zuo, *et al.*³⁸ They used a long, upright cylinder as an indenter (compared to the thin disc that we used). They found, as we did, that $f(\delta)$ matched the value expected for a clean fluid interface, except that in their case the particle raft changed the effective contact angle on the rod. They attributed the fluid-like response to dilation of the raft, and here we showed by imaging how the azimuthal compression is accommodated. Unlike the present case, however, the cylinder-indentation experiments always found a higher f for rafts than for a clean interface. We believe this difference arises because our disc has a pinned contact line, while the upright cylinder has a constant-angle boundary and the contact angle changes with the particles.

Jambon-Puillet, *et al.*⁴⁴ investigated collapse and sinking of particle rafts at fluid interfaces and found a dependence of (effectively) maximum indentation on the “effective weight” of the particles. In our experiments, the effective weight ranged from a minimum of 0.3 for acrylic at air-water to a maximum of 8 for polystyrene at oil-water. Our results do not follow the earlier trend, though; instead we found that the Teflon particles at air-water interfaces have a medium value of effective weight (~ 0.6 , compared to) but the greatest δ_{max} because of their greater hydrophobicity, and hence greater effectiveness at preventing the interface from touching the indenter.

We can compare particulate films to continuum-elastic films by comparing our results those of Box, *et al.*,³⁴ who related $df/d\delta$ to the dimensionless “bendability” parameter, τ , that compares bending stress to interfacial tension. (Large τ corresponds to small bending modulus.) To compare our results to theirs, we obtain an estimate of the rafts’ bending modulus from prior results,³⁰ which indicates that τ in a raft simplifies to approximately l/a . In our experiments, this ratio ranged from 1.7 (water-air) to 12 (oil mixture-water). We compared the numerical values of $df/d\delta$ where our parameter regimes overlapped: $R_{in}/l_c = 1.1$ and $\tau = 1.7$. Their predicted stiffness for continuum sheets (their K_1/γ) was about 7.1γ before the wrinkling instability, consistent with their measurements. From the best-fit to our experimental 2nd-plateau data we found 12.3γ , which is reasonably close to but nonetheless distinguishable from the continuum result. It is hard to be sure, though, whether this difference is real or is attributable to uncertainty in estimating the bending modulus of a particle raft. Perhaps more important, from the continuum theory³⁴ we would anticipate that the bending modulus and τ should affect $df/d\delta$ in this regime, which we did not observe in rafts. It therefore appears that the parameter scaling for rafts may be different for continuum systems. A possible explanation is that rafts appear to undergo the in-plane star-shaped deformation at an indentation that is far smaller than the critical δ for wrinkling in continuum sheets (which is $>20\times$ greater than the sheet thickness).

Although our experiments were performed on millimeter-scale particles, our results for the second plateau do not depend on particle size, so that these conclusions should apply to a monolayer of micron- or nanometer-sized particles. The range of δ in which the first plateau appears, however, is

probably limited to the particle diameter whereas the maximum indentation scale is set by l_c , so that the first plateau might be correspondingly less important as a decreases to the micron scale or smaller. The micro- to nanometer size range is more relevant for Pickering emulsions, and our results suggest that the particles could provide more effective stabilization than surfactants under some conditions, because of the greater maximum indentation depth shown in Fig. 6. For the same reason, liquid marbles or planar interfaces coated with particle rafts should be able to support heavier objects than clean interfaces, which may be useful in fluidic assembly processes.⁴⁶

Acknowledgments

We thank Benny Davidovitch and Greg Grason for helpful comments throughout this project. This research was supported in part by a grant from BP/The Gulf of Mexico Research Initiative through the C-MEDS consortium, and by the National Science Foundation (CBET-0967620 and CBET-1438425).

Conflicts of interests

The authors have no conflicts to declare.

References

- (1) Pike, N.; Richard, D.; Foster, W.; Mahadevan, L. *Proc. R. Soc. Lond. Ser. B-Biol. Sci.* **2002**, *269*, 1211-1215.
- (2) Mlot, N. J.; Tovey, C. A.; Hu, D. L. *Proc. Natl. Acad. Sci. U. S. A.* **2011**, *108*, 7669-7673.
- (3) Berton-Carabin, C. C.; Schroen, K. In *Annu. Rev. Food Sci. Technol., Vol 6*; Doyle, M. P., Klaenhammer, T. R., Eds.; Annual Reviews: Palo Alto, 2015; Vol. 6; pp 263-297.
- (4) Tavernier, I.; Wijaya, W.; Van der Meeren, P.; Dewettinck, K.; Patel, A. R. *Trends Food Sci. Technol.* **2016**, *50*, 159-174.
- (5) Bhargava, A.; Francis, A. V.; Biswas, A. K. *J. Colloid Interface Sci.* **1978**, *64*, 214-227.
- (6) Pickering, S. U. *J. Chem. Soc.* **1907**, *91*, 2001-2021.
- (7) Koretsky, A. F.; Kruglyakov, P. M. I. *Izv. Sib. Otd. Akad. Nauk. SSSR Ser. Khim. Nauk.* **1971**, *2*, 139-141.
- (8) Pieranski, P. *Phys. Rev. Lett.* **1980**, *45*, 569-572.
- (9) Lin, Y.; Skaff, H.; Emrick, T. S.; Dinsmore, A. D.; Russell, T. P. *Science* **2003**, *299*, 226.
- (10) Dinsmore, A. D.; Hsu, M. F.; Nikolaidis, M. G.; Marquez, M.; Bausch, A. R.; Weitz, D. A. *Science* **2002**, *298*, 1006.
- (11) Sun, J.; Zheng, X. L. *J. Env. Monitoring* **2009**, *11*, 1801-1809.
- (12) Katepalli, H.; John, V. T.; Bose, A. *Langmuir* **2013**, *29*, 6790-6797.
- (13) Saha, A.; Nikova, A.; Venkataraman, P.; John, V. T.; Bose, A. *ACS Appl. Mater. Interfaces* **2013**, *5*, 3094-3100.
- (14) Howard, B. C. In *National Geographic*, 2015.
- (15) Binks, B. P.; Murakami, R. *Nat. Mater.* **2006**, *5*, 865.
- (16) Illy, E.; Navarini, L. *Food Biophys.* **2011**, *6*, 335-348.
- (17) Aussillous, P.; Quere, D. *Nature* **2001**, *411*, 924-927.
- (18) Jin, J.; Ooi, C. H.; Dao, D. V.; Nguyen, N. T. *Micromachines* **2017**, *8*.
- (19) Marty, G.; Tsapis, N. *Eur. Phys. J. E* **2008**, *27*, 213-219.
- (20) Cui, M. M.; Emrick, T.; Russell, T. P. *Science* **2013**, *342*, 460-463.
- (21) Zoueshtiagh, F.; Baudoin, M.; Guerrin, D. *Soft Matter* **2014**, *10*, 9403-9412.
- (22) Li, X. G.; Xue, Y. H.; Lv, P. Y.; Lin, H.; Du, F.; Hu, Y. Y.; Shen, J.; Duan, H. L. *Soft Matter* **2016**, *12*, 1655-1662.
- (23) Aveyard, R.; Clint, J. H.; Nees, D.; Paunov, V. N. *Langmuir* **2000**, *16*, 1969-1979.

- (24) Bordacs, S.; Agod, A.; Horvolgyi, Z. *Langmuir* **2006**, *22*, 6944-6950.
- (25) Monteux, C.; Jung, E.; Fuller, G. G. *Langmuir* **2007**, *23*, 3975-3980.
- (26) Cicuta, P.; Vella, D. *Phys. Rev. Lett.* **2009**, *102*, 138302.
- (27) Leahy, B. D.; Pocivavsek, L.; Meron, M.; Lam, K. L.; Salas, D.; Viccaro, P. J.; Lee, K. Y. C.; Lin, B. H. *Phys. Rev. Lett.* **2010**, *105*, 058301.
- (28) Kassuga, T. D.; Rothstein, J. P. *J. Colloid Interface Sci.* **2015**, *448*, 287-296.
- (29) Jambon-Puillet, E.; Josserand, C.; Protiere, S. *Phys. Rev. Mater.* **2017**, *1*.
- (30) Vella, D.; Aussillous, P.; Mahadevan, L. *Europhys. Lett.* **2004**, *68*, 212-218.
- (31) Planchette, C.; Lorenceau, E.; Bianche, A. L. *Soft Matter* **2012**, *8*, 2444-2451.
- (32) Petit, P.; Bianche, A. L.; Lorenceau, E.; Planchette, C. *Phys. Rev. E* **2016**, *93*, 042802.
- (33) Huang, J.; Juskiewicz, M.; de Jeu, W. H.; Cerda, E.; Emrick, T.; Menon, N.; Russell, T. P. *Science* **2007**, *317*, 650-653.
- (34) Box, F.; Vella, D.; Style, R.; Neufeld, J. A. *Proc. R. Soc. A-Math. Phys. Eng. Sci.* **2017**, *473*, 20170335.
- (35) Holmes, D. P.; Crosby, A. J. *Phys. Rev. Lett.* **2010**, *105*, 038303.
- (36) Vella, D.; Huang, J.; Menon, N.; Russell, T. P.; Davidovitch, B. *Phys. Rev. Lett.* **2015**, *114*, 014301.
- (37) Vella, D.; Davidovitch, B. *Phys. Rev. E* **2018**, *98*, 013003.
- (38) Zuo, P. C.; Liu, J. L.; Li, S. P. *Soft Matter* **2017**, *13*, 2315-2321.
- (39) Nicolson, M. M. *Proc. Cambridge Phil. Soc.* **1949**, *45*, 288-295.
- (40) Vella, D.; Mahadevan, L. *Am. J. Phys.* **2005**, *73*, 817.
- (41) Keller, J. B. *Phys. Fluids* **1998**, *10*, 3009-3010.
- (42) He, W.; Senbil, N.; Dinsmore, A. D. *Soft Matter* **2015**, *11*, 5087-5094.
- (43) Du, K.; Glogowski, E.; Emrick, T.; Russell, T. P.; Dinsmore, A. D. *Langmuir* **2010**, *26*, 12518-12522.
- (44) Jambon-Puillet, E.; Josserand, C.; Protiere, S. *Langmuir* **2018**, *34*, 4437-4444.
- (45) Bormashenko, E.; Whyman, G.; Gendelman, O. *Adv. Condens. Matter Phys.* **2015**, *2015*, 206578.
- (46) Knuesel, R. J.; Jacobs, H. O. *Proc. Natl. Acad. Sci. U. S. A.* **2010**, *107*, 993-998.